Modeling of Cross-Coupling Magnetic Saturation in Signal-Injection-Based Sensorless Control of Permanent-Magnet Brushless AC Motors

Y. Li, Z. Q. Zhu, D. Howe, and C. M. Bingham

Department of Electronic and Electrical Engineering, University of Sheffield, Sheffield S1 3JD, U.K.

An improved brushless AC motor model is proposed for use in signal-injection-based sensorless control schemes by accounting for cross-coupling magnetic saturation between the d- and q-axes. The incremental self- and mutual-inductance characteristics are obtained by both finite-element analysis and measurements, and have been successfully used to significantly reduce the error in the rotor position estimation of sensorless control.

***Index Terms*—Brushless AC motor, cross-coupling effect, sensorless, signal injection.**

I. Introduction

SENSORLESS control of permanent-magnet (PM) brushless AC (BLAC) motors is desirable in order to reduce the system complexity and cost, and to improve reliability. Unlike other sensorless control methods whose performance is problematic during starting and low-speed operation, signal-injection-based sensorless schemes exhibit excellent control performance at standstill and low speeds. However, it was found experimentally in [1] that the error in the estimated rotor position increases with the load current, while in [2] it was shown that a significant error can arise due to the influence of cross-coupling magnetic saturation between the d- and q-axes. Although the effect of magnetic saturation on the cross coupling in permanent-magnet brushless machines is well known [3], it is generally neglected in the implementation of signal-injection-based sensorless control [1], [4].

This paper, therefore, presents a simple way to account for the cross-coupling effect. Incremental self- and mutual-inductance characteristics for use in an improved BLAC motor model are obtained by both finite-element analysis and measurements. They are subsequently used in a signal-injection-based sensorless control scheme and a significant reduction in the error in the estimated rotor position is achieved.

II. Modeling of Cross-Coupling Effect in BLAC Motor

When cross coupling between the d- and q-axes is considered, the voltage equations of a BLAC motor in the rotor reference dq-axis frame are [3]

$$\begin{bmatrix} v_d \\ v_q \end{bmatrix} = \begin{bmatrix} R_s + L_{dh}p & -\omega_r L_q + L_{dqh}p \\ \omega_r L_d + L_{qdh}p & R_s + L_{\mathrm{qh}}p \end{bmatrix} \begin{bmatrix} i_d \\ i_q \end{bmatrix} + \begin{bmatrix} 0 \\ \omega_r \psi_m \end{bmatrix} \tag{1}$$

where v_d, v_q, i_d, i_q, L_d, and L_q are the d- and q-axis voltages, currents, and apparent self-inductances, respectively, and L_{dh}, L_{qh}, L_{dqh}, and L_{qdh} are the incremental d– and q-axis self and mutual inductances, respectively. R_s is the phase resistance, ψ_m is the flux-linkage due to the permanent magnets, ω_r is the angular rotational speed, and $p = d/dt$.

High-frequency signal injection components in (1) can be approximated by

$$\begin{bmatrix} v_{dh} \\ v_{qh} \end{bmatrix} \approx \begin{bmatrix} L_{dh} & L_{dqh} \\ L_{qdh} & L_{qh} \end{bmatrix} \cdot p \begin{bmatrix} i_{dh} \\ i_{qh} \end{bmatrix} \tag{2}$$

where v_{dh}, v_{qh}, i_{dh} and i_{qh} are the high-frequency components of the d- and q-axis voltages and currents, respectively.

If the high-frequency signal, $v_{\mathrm{sig}} = V_{\mathrm{sig}} \sin(2\pi f_{\mathrm{HF}} t)$, is injected in the d-axis, the error in the estimated rotor position, $\Delta\theta$, can be calculated as

$$\Delta\theta \approx k_{\Delta\theta} \cdot \left[i^e_{qh} + (L_{dqh}/L_{qh}) i^e_{dh} \right] \tag{3}$$

where i^e_{dh}, i^e_{qh} are the high-frequency components of the estimated d- and q-axis currents, $k_{\Delta\theta} = (p(L^2_{\mathrm{avg}} - L^2_{\mathrm{dif\_}c})/ - 2v_{\mathrm{sig}}(L_{\mathrm{dif}} + L^2_{dqh}/L_{qh}))$, $L_{\mathrm{avg}} = (L_{qh} + L_{dh})/2$, $L_{\mathrm{dif}} = (L_{qh} - L_{dh})/2$, and $L^2_{\mathrm{dif\_}c} = L^2_{\mathrm{dif}} + L^2_{dqh}$.

When $[i^e_{qh} + (L_{dqh}/L_{qh}) i^e_{dh}]$ in (3) is controlled to be zero, the error in the estimated rotor position will be zero. Therefore, the accuracy of the parameters L_{dqh} and L_{qh} directly affects the rotor position estimation accuracy. Due to magnetic saturation, L_{dqh} and L_{qh} both vary with i_d and i_q. The variation can be obtained by either finite-element analysis or measurements.

III. Predicted and Measured Incremental Self and Mutual Inductances

L_{dh}, L_{qh}, L_{dqh}, and L_{qd}, are defined as

$$\begin{cases} L_{dh} = \partial\psi_d/\partial i_d, & L_{dqh} = \partial\psi_d/\partial i_q \\ L_{qdh} = \partial\psi_q/\partial i_d, & L_{qh} = \partial\psi_q/\partial i_q \end{cases} \tag{4}$$

where ψ_d and ψ_q are the d- and q-axis flux linkages. The finite-element predicted incremental self and mutual inductances are determined according to

$$\begin{cases} L_{dh} = [\psi_d(i_d + \Delta i_d, i_q, \Phi_m) - \psi_d(i_d, i_q, \Phi_m)]/\Delta i_d \\ L_{qh} = [\psi_q(i_d, i_q + \Delta i_q, \Phi_m) - \psi_q(i_d, i_q, \Phi_m)]/\Delta i_q \\ L_{dqh} = [\psi_d(i_d, i_q + \Delta i_q, \Phi_m) - \psi_d(i_d, i_q, \Phi_m)]/\Delta i_q \\ L_{qdh} = [\psi_q(i_d + \Delta i_d, i_q, \Phi_m) - \psi_q(i_d, i_q, \Phi_m)]/\Delta i_d \end{cases} \tag{5}$$

where Φ_m is the flux linkage due to permanent magnets.

Practically, the d- and q-axis incremental self and mutual inductances are measured indirectly from the high-frequency currents, $i^I_{dh}, i^I_{qh}, i^{II}_{dh}$, and i^{II}_{qh}, which flow when the high-frequency voltage v_{sig} is applied to the d- and q-axes [5]. i^I_{dh} and i^I_{qh} are

Digital Object Identifier 10.1109/TMAG.2007.892319

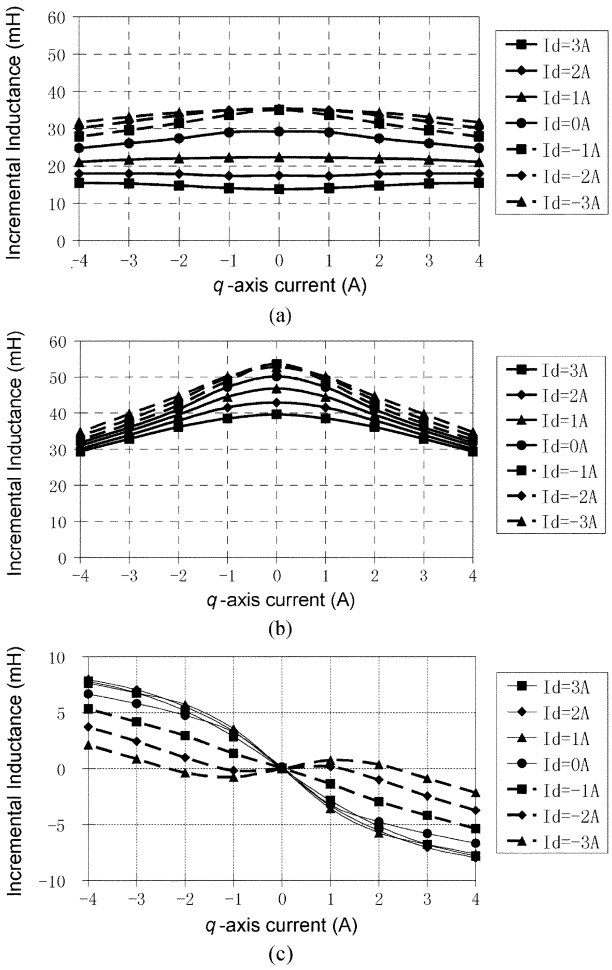

Fig. 1. Finite-element predicted incremental self and mutual inductances. (a)d-axis incremental inductance, L_{dh} (b) q-axis incremental inductance, L_{qh} (c) dq-axis incremental mutual inductances, L_{dqh} and L_{qdh}.

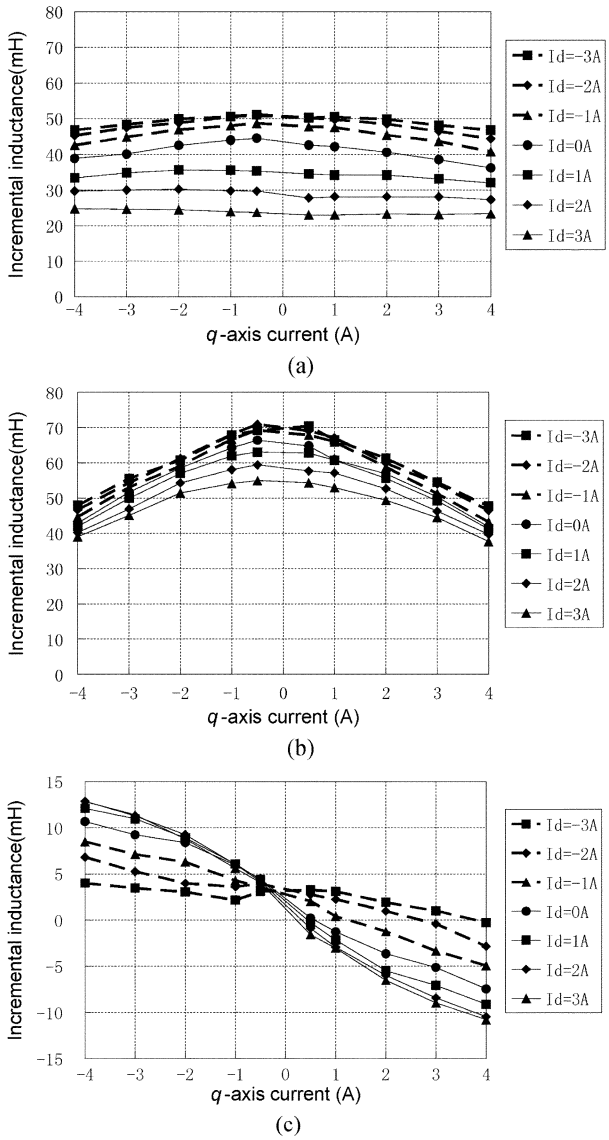

Fig. 2. Measured incremental self and mutual inductances. (a) d-axis incremental inductance, L_{dh} (b) q-axis incremental inductance, L_{qh} (c) dq-axis incremental mutual inductances, L_{dqh} and L_{qdh}.

the high-frequency components of the d- and q-axis currents, which result when v_{sig} is applied to the d-axis, i.e., $v_{dh} = v_{\text{sig}}$, when the BLAC motor is driven with its actual rotor position being measured via an encoder, while i_{dh}^{II} and i_{qh}^{II} are high-frequency components of the d- and q-axis currents when v_{sig} is applied to the q-axis, i.e., $v_{qh} = v_{\text{sig}}$, Therefore, from (2)

$$\begin{bmatrix} v_{\text{sig}} & 0 \\ 0 & v_{\text{sig}} \end{bmatrix} = \begin{bmatrix} L_{dh} & L_{dqh} \\ L_{qdh} & L_{qh} \end{bmatrix} \cdot p \begin{bmatrix} i_{dh}^{I} & i_{dh}^{II} \\ i_{qh}^{I} & i_{qh}^{II} \end{bmatrix} \tag{6}$$

and, hence

$$\begin{bmatrix} L_{dh} & L_{dqh} \\ L_{qdh} & L_{qh} \end{bmatrix} = \frac{1}{2\pi f_{\text{HF}}} \begin{bmatrix} v_{\text{sig}} & 0 \\ 0 & v_{\text{sig}} \end{bmatrix} \begin{bmatrix} i_{dh}^{I} & i_{dh}^{II} \\ i_{qh}^{I} & i_{qh}^{II} \end{bmatrix}^{-1} \tag{7}$$

where f_{HF} is the frequency of v_{sig}.

The 2-D finite element predicted and measured varation of the incremental self and mutual inductances with both i_d and i_q are shown in Figs. 1 and 2, respectively, for a six-pole BLAC motor which has an interior PM rotor, its rated speed, torque, and current being 1000 rpm, 4.0 Nm, and 4.0 A, respectively. As will be seen, the predictions compare well with measurements. However, the predicted values are somewhat smaller than the measured results due to the neglect of end effects, dimensional tolerances and uncertainties in the localized B–H characteristics of the stator and rotor laminations, as well as the influence of eddy currents. However, as will be evident from (3), and also Section IV, it is the ratio L_{dqh}/L_{qh} which determines the accuracy of the rotor position estimation.

IV. Measurement of Error in Estimated Rotor Position

From (3), both L_{dqh} and L_{qh} are required to determine the error in the estimated rotor position in a signal-injection-based sensorless control scheme. Fig. 3 compares finite-element predicted and measured ratios of L_{dqh}/L_{qh}, deduced from Figs. 1 and 2, respectively. As can be seen, although the predicted incremental inductances are smaller than the measured values, the predicted and measured ratios of L_{dqh}/L_{qh} agree well. Hence, either can be used to improve the accuracy of the estimated rotor position. However, interpolation to account for the fact that the incremental inductances vary with both i_d and i_q is too complex to implement on a DSP. Therefore, much simpler approxi-

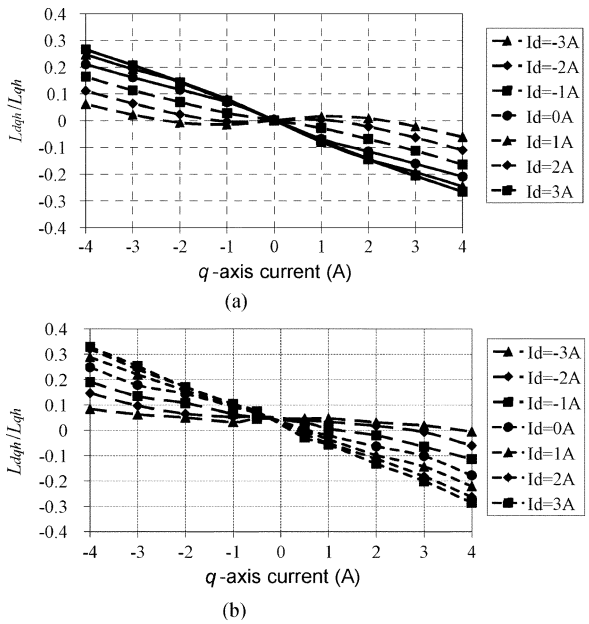

Fig. 3. Comparison of predicted and measured ratio of L_{dqh}/L_{qh}. (a) Predicted. (b) Measured.

mation functions are used to represent the variation in the ratio L_{dqh}/L_{qh}, viz.

$$\frac{L_{dqh}}{L_{qh}} = \begin{cases} k_1 \cdot i_q^e, & i_d^e \geqslant 0 \\ (k_1 + k_2 i_d^e) \cdot i_q^e, & i_d^e < 0 \end{cases} \tag{8}$$

where k_1, and k_2 are constant coefficients. For the machine under consideration, $k_1 = -0.050\ \mathrm{A}^{-1}$, $k_2 = -0.009\ \mathrm{A}^{-2}$ from finite-element analysis predictions, while the values deduced from measurements are $k_1 = -0.060\ \mathrm{A}^{-1}, k_2 = -0.011\ \mathrm{A}^{-2}$.

The proposed signal-injection-based sensorless control scheme remains essentially similar to that described in [4] in which dq-axis cross coupling was neglected. However, the error in the estimated rotor position, which is calculated by (3), is now considered. The scheme is implemented on a TMS320C31 DSP, and a precision encoder is used to measure the actual rotor position, and enable the error to be determined. The frequency of the AD sampling, the control loop, and the PWM are all 5 kHz, and the injected sinusoidal voltage is 35 V, 330 Hz.

As shown in Fig. 4(a), when conventional signal-injection-based sensorless control is employed, i.e., L_{dqh}/L_{qh} is neglected, the error in the estimated rotor position can be large, and depends on both i_d and i_q, the average error in the motor under consideration being 15.4°. When dq-axis cross coupling is accounted for, the accuracy of the estimated rotor position is improved significantly, as shown in Fig. 4(b) and (c). For example, the average errors are reduced to 2.4° and 1.5°, respectively, when the finite-element predicted and measured L_{dqh}/L_{qh}, Fig. 3(a) and (b), are employed, the error being slightly smaller when the measured L_{dqh}/L_{qh} is used since it accounts for the end-winding inductances.

V. Conclusion

An improved implementation of high-frequency signal injection sensorless control of a BLAC motor, which accounts for cross-coupling magnetic saturation between the d- and q-axes, has been demonstrated. The required parameters are obtained by either finite-element analysis or from measurements. It has been shown that the error in the estimated rotor position can be reduced significantly.

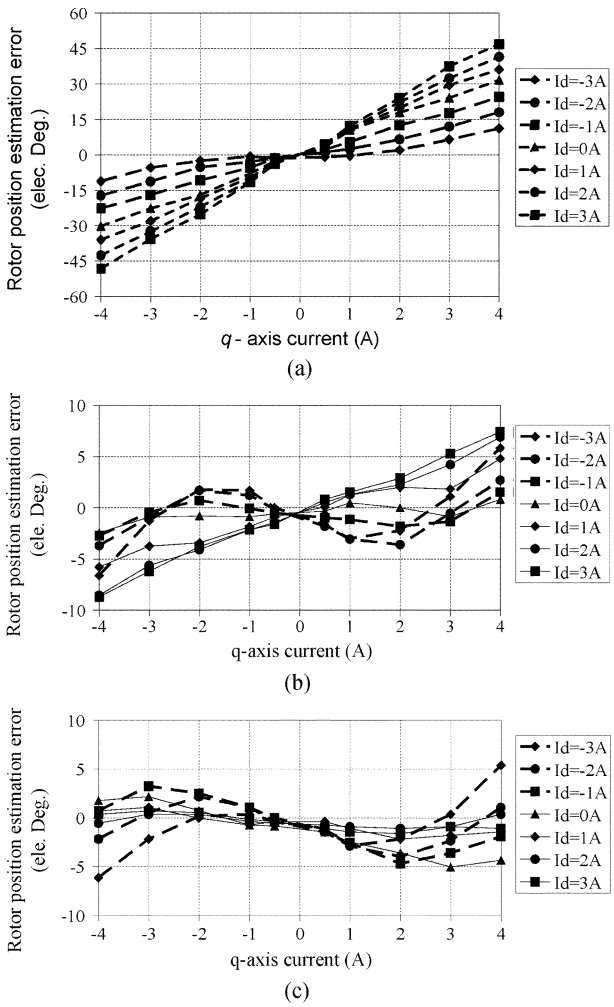

Fig. 4. Measured error in estimated rotor position. (a) Neglecting $L_{dqh}/L_{qh}, \mathrm{avg}(|\theta_r^e - \theta_r|) = 15.4°$. (b) Using finite-element calculated $L_{dqh}/L_{qh}, \mathrm{avg}(|\theta_r^e - \theta_r|) = 2.4°$. (c) Using measured $L_{dqh}/L_{qh}, \mathrm{avg}(|\theta_r^e - \theta_r|) = 1.5°$.

References

[1] M. J. Corley and R. D. Lorenz, "Rotor position and velocity estimation for a salient-pole permanent magnet synchronous machine at standstill and high speed," *IEEE Trans. Ind. Appl.*, vol. 34, no. 4, pp. 784–789, Jul.–Aug. 1998.

[2] P. Guglielmi, M. Pastorelli, and A. Vagati, "Cross saturation effects in IPM motors and related impact on zero-speed sensorless control," *Conf. Rec. IEEE-IAS Annu. Meeting*, vol. 4, pp. 2546–2552, 2005.

[3] B. Stumberger, G. Stumberger, D. Dolinar, A. Hamler, and M. Trlep, "Envaluation of saturation and cross-magnetization effects in interior permanent-magnet synchronous motor," *IEEE Trans. Ind. Appl.*, vol. 39, no. 5, pp. 1264–1271, Sep.–Oct. 2003.

[4] J. H. Jang, S. K. Sul, J. I. Ha, K. Ide, and M. Sawamura, "Sensorless drive of surface-mounted permanent-magnet motor by high-frequency signal injection based on magnetic saliency," *IEEE Trans. Ind. Appl.*, vol. 39, no. 4, pp. 1031–1039, Jul.–Aug. 2003.

[5] S. Ogasawara and H. Akagi, "Implementation and position control performance of a position-sensorless IPM motor drive system based on magnetic saliency," *IEEE Trans. Ind. Appl.*, vol. 34, no. 4, pp. 806–812, Jul.–Aug. 1998.

Manuscript received January 30, 2007 (e-mail: Z.Q.Zhu@sheffield.ac.uk).